Nanoparticle Morphology Hot Paper

Deutsche Ausgabe: DOI: 10.1002/ange.201504099
Internationale Ausgabe: DOI: 10.1002/anie.201504099

Sequential Anion and Cation Exchange Reactions for Complete Material Transformations of Nanoparticles with Morphological Retention**

*James M. Hodges, Karel Kletetschka, Julie L. Fenton, Carlos G. Read, and Raymond E. Schaak**

Abstract: *Ion exchange reactions of colloidal nanocrystals provide access to complex products that are synthetically challenging using traditional hot-injection methods. However, such reactions typically achieve only partial material transformations by employing either cation or anion exchange processes. It is now shown that anion and cation exchange reactions can be coupled together and applied sequentially in one integrated pathway that leads to complete material transformations of nanocrystal templates. Although the product nanocrystals do not contain any of the original constituent elements, the original morphology is retained, thereby fully decoupling morphology and composition control. The sequential anion/cation exchange process was applied to pseudospherical CdO nanocrystals and ZnO tetrapods, producing fully transformed and shape-controlled nanocrystals of copper and silver sulfides and selenides. Furthermore, hollow core–shell tetrapod ZnS@CdS heterostructures were readily accessible.*

The size- and shape-dependent characteristics of nanoscale materials make them ideal systems for studying structure–property relationships while simultaneously providing a platform for tuning physical and chemical properties.[1–5] Accordingly, synthetic procedures for generating nanoparticles must permit the precise control of morphology and uniformity. Hot-injection methods, where organometallic or metal–organic precursors are heated in the presence of surfactants, are among the most effective techniques for synthesizing high-quality monodisperse colloidal nanoparticles.[6,7] However, the direct synthesis of nanocrystals using this approach requires a precise balance between crystal nucleation, particle growth,[8,9] and the redox potential of the chemical reagents, as well as surface-stabilizing agents for preferentially exposing certain crystal facets.[10] Consequently, many important material systems are not accessible as monodisperse and/or shape-controlled colloidal nanoparticles. One way to circumvent this problem and gain access to synthetically challenging nanomaterials is to employ post-synthetic modifications to nanocrystal templates that are preprogrammed with a desired characteristic, such as size or shape.[11–14] Ion exchange reactions, where the cation or anion sublattice of a preformed nanocrystal is replaced with different ions, are emerging as powerful alternatives to high-temperature injection methods for producing high-quality nanocrystals with unprecedented uniformity and shape control in synthetically challenging systems.[15–22] Furthermore, ion exchange chemistry has been shown to be an effective method for transforming preformed nanocrystal templates into more complex heterostructures, such as core–shell nanoparticles,[23,24] providing additional levers for tuning material properties.

As the applications for monodisperse colloidal nanocrystals continue to mature, their size and shape requirements are becoming more rigid, and there is a need for new synthetic methods that can more rigorously and predictably control these parameters across a broad range of material systems. Current nanoscale ion-exchange methods have been limited to partial material transformations, involving either anion or cation exchange, which ultimately restricts the method to specific subclasses of materials, such as metal sulfides. Complete material transformations involving sequential anion and cation exchange could offer significant opportunities for preprogramming morphology and, consequently, desired physical and chemical properties across diverse subclasses of nanomaterials. Such an approach would, in effect, completely decouple morphology control from the targeted composition and structure.

Herein, we show that nanocrystal anion and cation exchange reactions can be applied sequentially in an integrated reaction scheme to achieve complete material transformations of preformed metal oxide nanocrystals into chalcogenide nanocrystals of different metals with morphological retention (Figure 1). The product nanocrystals, therefore, consist entirely of elemental components not found in the original material, yet the morphologies and uniformities

[*] J. M. Hodges, K. Kletetschka, J. L. Fenton, C. G. Read, Prof. R. E. Schaak
Department of Chemistry and Materials Research Institute
The Pennsylvania State University
University Park, PA 16802 (USA)
E-mail: res20@psu.edu

[**] This work was supported by the U.S. National Science Foundation (DMR-1305564). TEM imaging was performed at the Materials Characterization Lab of the Penn State Materials Research Institute.

Supporting information for this article is available on the WWW under http://dx.doi.org/10.1002/anie.201504099.

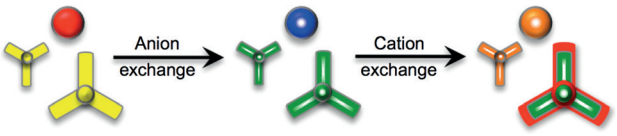

Figure 1. Schematic representation of the complete material transformation of shape-controlled metal oxide nanocrystals into chalcogenide nanocrystals of different metals using a sequential anion/cation exchange process. Anion exchange produces Kirkendall voids, and partial cation exchange can be implemented in the final step to access core–shell heterostructures.

of the initial nanocrystal templates are conserved. The anion sublattice is exchanged first, followed by the cation sublattice, using reactions that are driven by the chemical reactivity of the anion precursor and the affinity of the ligand for the cation in the metal oxide. Anion exchange was targeted first because metal oxide nanocrystals are known to react with chalcogen reagents to form chalcogenides[22] and also because of the slow reaction kinetics of cation exchange reactions involving metal oxide nanocrystals, which can lead to core–shell structures.[25] However, different exchange sequences may be effective with other material transformations. The conversion of CdO into Cu_xS was used as a model system to demonstrate the complete material transformation. The approach was extended to other important material systems, ultimately incorporating several anion exchange (O→S, Se) and cation exchange (Cd→Cu, Ag; Zn→Cu) reactions into the integrated sequential processes. The morphologies of the original nanocrystals can be retained during application of these sequential modifications, allowing us to program a desired shape into the metal oxide nanotemplate, which is ultimately transferred to the final product. Furthermore, the anion/cation exchange sequence provides access to highly complex core–shell nanoparticles with unique architectures that cannot be achieved using conventional ion-exchange methods.

The CdO nanoparticle templates were synthesized by heating $[Cd(acac)_2]$ and oleic acid (OLAC) in 1-octadecene (ODE) to reflux (315 °C) for one hour (see the Supporting Information for details).[26] Figure 2a shows a transmission electron microscopy (TEM) image of the resulting pseudo-spherical nanoparticles, which have diameters of 16 ± 1 nm.

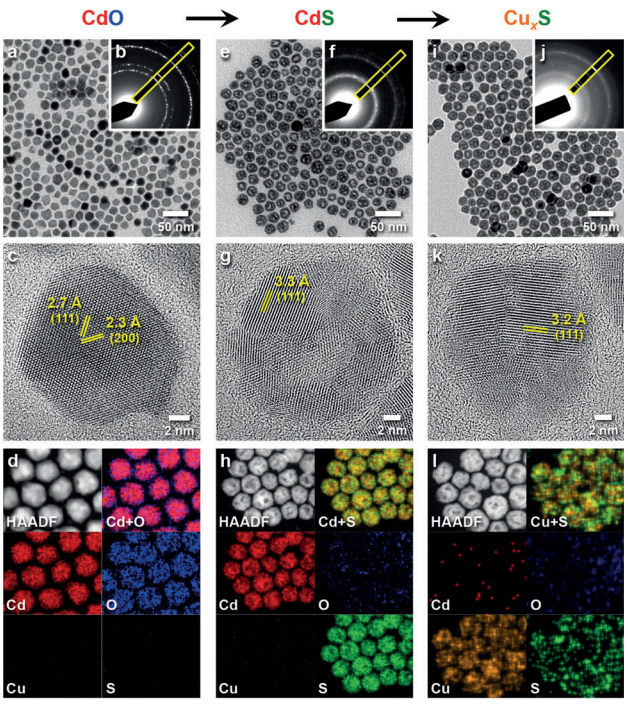

Figure 2. Representative TEM, SAED (with simulated data outlined in yellow), HRTEM, and STEM-EDS HAADF images with the corresponding EDS elemental maps of a–d) CdO nanoparticles, e–h) hollow CdS nanoparticles, and i–l) hollow Cu_xS nanoparticles.

The selected area electron diffraction (SAED) pattern in Figure 2b and the powder X-ray diffraction (XRD) patterns in Figure 3a confirm the formation of rock-salt-type CdO

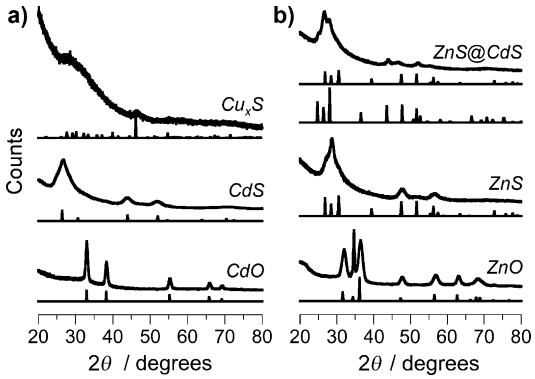

Figure 3. Powder XRD patterns for a) CdO, hollow CdS, and hollow Cu_xS nanoparticles and b) ZnO tetrapods, hollow ZnS tetrapods, and ZnS@CdS core–shell tetrapods. Simulated XRD patterns are shown for comparison; for the ZnS@CdS sample, the two simulated patterns correspond to wurtzite-type ZnS (top) and wurtzite-type CdS (bottom).

nanocrystals without any observable crystalline impurities. A corresponding high-resolution TEM (HRTEM) image, shown in Figure 2c, reveals lattice spacings of 2.7 Å that are characteristic of the (111) plane of CdO. As the first step towards a complete material transformation process, the CdO nanoparticles were converted into CdS by anion exchange using $[(CH_3)_3Si]_2S$ as a reactive sulfide anion source. Briefly, the CdO nanoparticles were heated to 130 °C in trioctylphosphine oxide (TOPO), and then a solution of $[(CH_3)_3Si]_2S$ in trioctylphosphine (TOP) was slowly added. Both the SAED (Figure 2f) and XRD (Figure 3a) patterns confirm the formation of zinc-blende-type CdS and the absence of the CdO precursor. A TEM image of the CdS nanoparticle product (Figure 2e) indicates that the pseudo-spherical shape of the CdO precursor is retained. However, the particles now contain a central void that results from a nanoscale Kirkendall effect, which is well known for nanoparticle diffusion and exchange reactions involving metal oxides and chalcogenides.[27] Because of the hollow center, the average diameter of the CdS nanoparticle product increases to 21 ± 2 nm. The corresponding HRTEM image (Figure 2g) shows lattice spacings of 3.3 Å that are consistent with the (111) plane of zinc-blende-type CdS. As both rock-salt-type CdO and zinc-blende-type CdS contain a cubic close-packed array of Cd atoms, it is conceivable that the structure of the cation sublattice was preserved during the anion exchange reaction, resulting in the formation of zinc-blende-type CdS rather than wurtzite-type CdS.

As the final step of the complete material transformation process, the hollow CdS nanoparticles were converted into Cu_xS using a cation exchange reaction. Briefly, a toluene dispersion of the CdS nanoparticles was added to a methanol solution of $[Cu(CH_3CN)_4]PF_6$, inducing an immediate color change from yellow to brown, which is indicative of the conversion of CdS into Cu_xS.[28] Powder XRD data (Figure 3a) of the resulting particles show no evidence of zinc-

blende-type CdS, indicating its complete consumption. The observed broad peaks match roughly with the simulated pattern for digenite-type $Cu_{1.8}S$, although this assignment cannot be made unambiguously given the broad peaks and the complexity of the Cu–S system. The corresponding SAED pattern (with a digenite-type $Cu_{1.8}S$ reference) in Figure 2j confirms the absence of CdS and the presence of Cu_xS. The TEM image in Figure 2i indicates that the pseudo-spherical hollow morphology of the CdS template nanoparticles is retained during the cation exchange process, and the HRTEM image in Figure 2k reveals lattice spacings of 3.2 Å that match with the (0015) plane of digenite-type $Cu_{1.8}S$, which has been observed in other nanostructured copper sulfide systems.[29,30] Whereas nanoparticle anion exchange reactions often result in the formation of hollow nanoparticles because of a significant difference between the outward and inward diffusion rates of the anionic species, cation exchange processes such as those used to transform CdS to Cu_xS typically do not.[18] The observation of the hollow center in the Cu_xS product is evidence that the cation exchange reaction that converts CdS into Cu_xS proceeds with morphological retention, indicating that morphological features can indeed be programmed into targeted nanoparticle products by multistep sequential anion and cation exchange processes.

Further evidence of the complete material exchange comes from element maps generated by scanning transmission electron microscopy coupled with energy dispersive spectroscopy (STEM-EDS; ensemble EDS data are included in the Supporting Information, Figure S2). Figure 2d shows a high-angle annular dark field (HAADF) STEM image of the CdO nanoparticle templates, along with the corresponding element maps for Cd and O. The STEM-EDS element maps for Cu and S, which show no signal above background as expected for CdO nanoparticles, are included as controls. Figure 2h shows a HAADF-STEM image of the CdS nanoparticles, confirming their hollow nature. The corresponding STEM-EDS element maps verify the colocalization of Cd and S and confirm that O is no longer present. Cu is again included as a background control. Figure 2l shows a HAADF-STEM image of the Cu_xS nanoparticles, which also confirms their hollow nature. The STEM-EDS element maps show that Cu and S are present in the Cu_xS nanoparticles while the signals for Cd and O have both returned to background levels. Taken together, the STEM-EDS data in Figure 2 validate the conclusion of complete material transformation that was drawn from the TEM, SAED, and XRD data.

Using CdO as a model template, other completely transformed nanoparticle products with different cations and anions can also be accessed. For example, Figure S2c shows XRD and TEM data indicating that the hollow CdS nanoparticles derived from the CdO nanoparticle templates can be transformed into Ag_2S upon cation exchange with $AgNO_3$ in methanol at room temperature. Similarly, the CdO template nanoparticles were anion-exchanged to form hollow CdSe nanoparticles upon reaction with a TOP solution of the selenide anion reagent $[(CH_3)_3Si]_2Se$ at 130 °C (Figure S2a). These zinc-blende-type CdSe hollow nanoparticles were readily converted into Cu_xSe using the same reagents and reaction conditions used to transform CdS into Cu_xS (Figure S2b). The successful transformation of CdO into Cu_xS, Ag_2S, and Cu_xSe provides compelling evidence that the application of sequential anion and cation exchange reactions is potentially general.

The above examples utilized pseudo-spherical CdO nanoparticles as templates, which rendered the products pseudo-spherical. To diversify both the accessible morphologies and the nanoparticle templates, we also explored sequential anion and cation exchange reactions on tetrapod-shaped ZnO nanoparticles synthesized by injecting an ODE solution of zinc stearate into 1-octadecanol at 250 °C. TEM images of ZnO tetrapods with average arm lengths of 7 nm are shown in Figures 4a and S3a. The higher contrast in the center of the

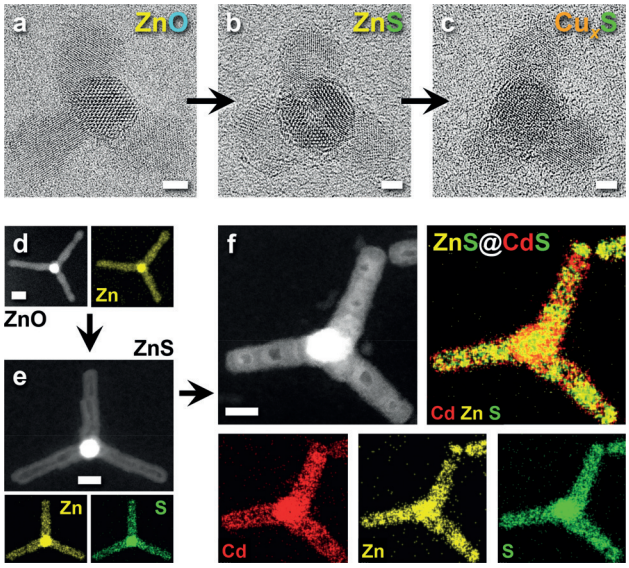

Figure 4. HRTEM images of small a) ZnO, b) ZnS, and c) Cu_xS tetrapods. STEM-HAADF images and corresponding EDS maps of larger d) ZnO tetrapods, e) ZnS tetrapods, and f) ZnS@CdS core–shell tetrapod heterostructures.

nanoparticles is consistent with a tetrapod arm extending perpendicular to the TEM grid, as is typically observed for transmission-mode projections of tetrapod-shaped nanoparticles.[31] Upon reaction with $[(CH_3)_3Si]_2S$ at 250 °C, the ZnO tetrapods are transformed into ZnS tetrapods, as shown in the TEM images in Figures 4b and S3b. Powder XRD data (Figure S3b) indicate the formation of wurtzite-type ZnS nanoparticles and the consumption of the ZnO precursor. Importantly, the tetrapod shape is conserved during the anion exchange reaction, and the formation of hollow voids in the arms of the single-crystal tetrapods is a unique morphological feature that is rarely encountered.[32]

To complete the transformation, the ZnS tetrapods with voids in each arm were reacted with a methanol solution of $[Cu(CH_3CN)_4]PF_6$ at room temperature, under similar conditions as for the conversion of CdS into Cu_xS. TEM, HRTEM, and HAADF-STEM images (Figures 4c, S3c, and S4) of the resulting nanoparticles show that the tetrapod shape programmed into the ZnS is retained during the cation

exchange process. Powder XRD data (Figure S3c) show the absence of wurtzite-type ZnS reflections and the presence of broad peaks that match with Cu_xS. The STEM-EDS element maps shown in Figure S4 confirm the morphology-conserving transformation from ZnO to ZnS and finally to Cu_xS. In particular, no Zn signal remains in the STEM-EDS element map of the Cu_xS particle, and there is a strong Cu signal localized on the nanoparticles shown in the corresponding HAADF-STEM image. The data therefore provide compelling evidence for a total material transformation of ZnO tetrapods into Cu_xS tetrapods.

We also explored the possibility of using combined anion/cation exchange reactions as a method for engineering nanomaterials with more sophisticated and intricate multicomponent architectures. Specifically, we synthesized ZnO tetrapods with longer 30 nm arms (Figure 4d) and then performed complete anion exchange to produce hollow ZnS tetrapods followed by partial cation exchange with Cd^{2+}. To accomplish the partial cation exchange, the 30 nm hollow ZnS tetrapods shown in Figures 4e and S5b were added to a Cd nonanoic acid complex at 210 °C and heated for three hours. The ZnS to CdS transition occurred significantly more slowly than the other exchange reactions, which was illustrated by a slow change from colorless to yellow over the course of three hours. Figures 4f and S5c show TEM images of the products, which retain the hollow tetrapod shape defined by the ZnS template. Powder XRD data shown in Figure 3b show reflections consistent with both wurtzite-type CdS and wurtzite-type ZnS. Importantly, the STEM-EDS element maps shown in Figure 4f clearly indicate that Cd and Zn are both present within the nanostructures. The Zn component falls within the silhouette of the Cd, which suggests a ZnS@CdS core–shell morphology. The formation of a nanostructurally complex hollow core–shell tetrapod-shaped nanocrystal underscores the diversity of the anion/cation exchange reaction sequence and opens the door to the programmed synthesis of other highly complex nanomaterials.

In conclusion, an integrated anion/cation exchange sequence can be used to achieve complete material transformations of metal oxide nanocrystals with morphological retention. This approach allows us to preprogram a desired morphology into metal oxide nanocrystals, and then arbitrarily transfer those characteristics to other material systems. Furthermore, this technique can be used to obtain unique multicomponent heterostructures that are not accessible using traditional methods. The ability to fully decouple morphology and composition control in nanocrystal synthesis is anticipated to provide new capabilities for designing and accessing high-quality colloidal nanostructures with precisely targeted features.

Keywords: anion exchange · cation exchange · Kirkendall effect · morphology · nanoparticles

How to cite: *Angew. Chem. Int. Ed.* **2015**, *54*, 8669–8672
Angew. Chem. **2015**, *127*, 8793–8796

[1] C. Burda, X. Chen, R. Narayanan, M. A. El-Sayed, *Chem. Rev.* **2005**, *105*, 1025.
[2] X. C. Ye, J. E. Collins, Y. Kang, J. Chen, D. T. N. Chen, A. G. Yodh, C. B. Murray, *Proc. Natl. Acad. Sci. USA* **2010**, *107*, 22430.
[3] Y. Jun, J. Choi, J. Cheon, *Angew. Chem. Int. Ed.* **2006**, *45*, 3414; *Angew. Chem.* **2006**, *118*, 3492.
[4] S. G. Kwon, T. Hyeon, *Acc. Chem. Res.* **2008**, *41*, 1696.
[5] Y. Xia, Y. Xiong, B. Lim, S. E. Skrabalak, *Angew. Chem. Int. Ed.* **2009**, *48*, 60; *Angew. Chem.* **2009**, *121*, 62.
[6] X. Peng, L. Manna, W. Yang, J. Wickham, E. Scher, A. Kradavanich, A. P. Alivisatos, *Nature* **2000**, *404*, 59.
[7] C. Wang, H. Daimon, Y. Lee, J. Kim, S. Sun, *J. Am. Chem. Soc.* **2007**, *129*, 6974.
[8] Y. Yin, A. P. Alivisatos, *Nature* **2005**, *437*, 664.
[9] S. G. Kwon, T. Hyeon, *Small* **2011**, *7*, 2685.
[10] J. Gao, C. M. Bender, C. J. Murphy, *Langmuir* **2003**, *19*, 9066.
[11] E. J. Popczun, C. G. Read, C. W. Roske, N. S. Lewis, R. E. Schaak, *Angew. Chem. Int. Ed.* **2014**, *53*, 5427; *Angew. Chem.* **2014**, *126*, 5531.
[12] Y. Yin, R. M. Rioux, C. K. Erdonmez, S. Hughes, G. A. Somorjai, A. P. Alivisatos, *Science* **2004**, *304*, 711.
[13] I. T. Sines, D. D. Vaughn II, A. J. Biacchi, C. E. Kingsley, E. J. Popczun, R. E. Schaak, *Chem. Mater.* **2012**, *24*, 3088.
[14] X. Xia, Y. Wang, A. Ruditskiy, Y. Xia, *Adv. Mater.* **2013**, *25*, 6313.
[15] D. H. Son, S. M. Hughes, Y. Yin, A. P. Alivisatos, *Science* **2004**, *306*, 1009.
[16] J. M. Luther, H. Zheng, B. Sadtler, A. P. Alivisatos, *J. Am. Chem. Soc.* **2009**, *131*, 16851.
[17] J. B. Rivest, P. K. Jain, *Chem. Soc. Rev.* **2013**, *42*, 89.
[18] S. Deka, K. Miszta, D. Dorfs, A. Genovese, G. Bertoni, L. Manna, *Nano Lett.* **2010**, *10*, 3770.
[19] H. Li, R. Brescia, M. Povia, M. Prato, G. Bertoni, L. Manna, *J. Am. Chem. Soc.* **2013**, *135*, 12270.
[20] S. Gupta, S. V. Kershaw, A. L. Rogach, *Adv. Mater.* **2013**, *25*, 6923.
[21] H. Zhang, L. V. Solomon, D. Ha, S. Honrao, R. G. Hennig, R. D. Robinson, *Dalton Trans.* **2013**, *42*, 12596.
[22] J. Park, H. Zheng, Y. Jun, A. P. Alivisatos, *J. Am. Chem. Soc.* **2009**, *131*, 13943.
[23] J. M. Pietryga, D. J. Werder, D. J. Williams, J. L. Casson, R. D. Schaller, V. I. Klimov, J. A. Hollingsworth, *J. Am. Chem. Soc.* **2008**, *130*, 4879.
[24] Q. A. Akkerman, A. Genovese, C. George, M. Prato, I. Moreels, A. Casu, S. Marras, A. Curcio, A. Scarpellini, T. Pellegrino, L. Manna, *ACS Nano* **2015**, *9*, 521.
[25] M. Sytnyk, R. Kirchschlager, M. I. Bodnarchuk, D. Primetzhofer, D. Kriegner, H. Enser, J. Stangl, P. Bauer, M. Voith, A. W. Hassel, F. Krumeich, F. Ludwig, A. Meingast, G. Kothleitner, M. V. Kovalenko, W. Heiss, *Nano Lett.* **2013**, *13*, 586.
[26] T. R. Gordon, T. Paik, D. R. Klein, G. V. Naik, H. Caglayan, A. Boltasseva, C. B. Murray, *Nano Lett.* **2013**, *13*, 2857.
[27] W. Wang, M. Dahl, Y. Yin, *Chem. Mater.* **2013**, *25*, 1179.
[28] P. K. Jain, L. Amirov, S. Aloni, A. P. Alivisatos, *J. Am. Chem. Soc.* **2010**, *132*, 9997.
[29] N. J. Freymeyer, P. D. Cunningham, E. C. Jones, B. J. Golden, A. M. Wiltrout, K. E. Plass, *Cryst. Growth Des.* **2013**, *13*, 4059.
[30] P. Leidinger, R. Popescu, D. Gerthsen, H. Lunsdorf, C. Feldmann, *Nanoscale* **2011**, *3*, 2544.
[31] D. J. Milliron, S. M. Hughes, Y. Cui, L. Manna, J. Li, L. Wang, A. P. Alivisatos, *Nature* **2004**, *430*, 190.
[32] A. E. Henkes, R. E. Schaak, *Inorg. Chem.* **2008**, *47*, 671.

Received: May 5, 2015
Published online: June 25, 2015